Transition from weak turbulence to collapse turbulence regimes in the Majda-McLaughlin-Tabak model

Ashleigh Simonis and Yulin Pan*

Department of Naval Architecture and Marine Engineering, University of Michigan, Ann Arbor, Michigan 48109, USA

(Received 28 February 2024; accepted 19 July 2024; published 5 August 2024)

It is well known that wave collapses can emerge from the focusing one-dimensional (1D) Majda-McLaughlin-Tabak (MMT) model as a result of modulational instability. However, how these wave collapses affect the spectral properties and statistics of the wave field has not been adequately studied. We undertake this task by simulating the forced-dissipated 1D MMT model over a range of forcing amplitudes. Our results show that when the forcing is weak, the spectrum agrees well with the prediction by wave turbulence theory with few collapses in the field. As the forcing strength increases, we see an increase in the occurrence of collapses, together with a transition from a power-law spectrum to an exponentially decaying spectrum. Through a spectral decomposition, we find that the exponential spectrum is dominated by the wave collapse component in the nonintegrable MMT model, which is in analogy to a soliton gas in integrable turbulence.

DOI: 10.1103/PhysRevE.110.024202

I. INTRODUCTION

Wave turbulence occurs in physical systems consisting of large ensembles of weakly interacting nonlinear dispersive waves. Wave turbulence theory (WTT) provides a statistical description of the behavior of these wave systems and has rich applications in many physical contexts such as plasma physics (e.g., Ref. [1]), physical oceanography (e.g., Ref. [2]), acoustics (e.g., Ref. [3]), and optics (e.g., Ref. [4]). The centerpiece of WTT is the so-called wave kinetic equation (WKE), which describes the evolution of the wave spectrum due to wave-wave interactions, and yields the Kolmogorov-Zakharov (KZ) spectra as stationary solutions [5]. Over the decades, many efforts (e.g., Refs. [6–14]) have been made to verify the WKE and KZ solutions in both numerical and experimental settings.

One model that holds a special position in the development of WTT verification is the Majda-McLaughlin-Tabak (MMT) model, which was introduced in 1997 in Ref. [15] as a testbed for WTT. In Ref. [15], it was found that the numerical simulation of the MMT equation yields a stationary spectrum that is significantly steeper than the KZ solution. Among several efforts to explain the discrepancy, Zakharov [16] argued that it may result from the existence of coherent structures in the wave field generated by the MMT model. In particular, it is shown in Refs. [16–18] that the defocusing MMT model allows the solution of quasisolitons, while the focusing MMT model allows wave collapses, i.e., finite-time high-amplitude singularities. In this paper, we adopt the terminology of focusing or defocusing nonlinearity [19] to refer to cases where the nonlinear and dispersive terms have the opposite or same sign, despite possible confusion in the context of the MMT model, as pointed out in Ref. [20]. However, Zakharov's argument is not widely accepted and the result of the MMT study [15] has remained unresolved within the wave turbulence community for many years. This was until recent studies [21,22] (also see Ref. [23]) for the defocusing MMT model. In particular, Ref. [21] argues that intermittency at high nonlinearity can lead to spectral anomaly compared to the KZ solution. Reference [22] clarifies that the width of the inertial range, a factor ignored in previous studies, must be sufficiently large for the KZ solution to be observed. This means that the inertial range realized in Ref. [15] (as well as in Ref. [21] as shown in the Appendix of Ref. [22]) is not wide enough. Further widening of the inertial range allows the spectrum to approach the KZ solution, regardless of the nonlinearity level and possible coherent structures. However, it remains unclear how the spectrum behaves in the focusing MMT model and whether wave collapses affect the spectral properties.

Generally speaking, wave collapses can be induced by modulational instability, resulting in the formation of a point singularity in finite time. At the time of a collapse, both the quadratic and quartic components of the Hamiltonian surge with the total Hamiltonian conserved, which prohibits collapses for defocusing nonlinearity. Although wave collapses and the mechanism for their formation are well studied in the nonlinear Schrödinger equations (NLS) (e.g., Ref. [24]), we highlight that the MMT model is susceptible to a different kind of instability. In Ref. [20] it was shown that the focusing MMT equation admits a modulational instability by short-wave modulations, i.e., the wavelength of the modulation is much smaller than that of the carrier wave, in contrast to the typical Benjamin-Feir instability. Wave collapses generated from a random wave field have been investigated in several studies (e.g., Refs. [16,17,19,20,25–27]), focusing on their effect on intermittency, energy transfer mechanisms, and inception of modulational instability. However, the nonlinearity level achieved in these studies is only moderately high, with random waves remaining the dominant feature and the

*Contact author: yulinpan@umich.edu

spectrum maintaining a power-law form (which is not the case with a further increase in nonlinearity, as we will show). The regime of wave collapses dominating the wave field at stronger nonlinearity has not been well understood.

In this work, we numerically study the focusing MMT dynamics in forced-dissipated simulations covering a broad range of nonlinearity levels, from a weak wave turbulence regime to a regime where wave collapses become dominant. At a low nonlinearity level, we find a wave turbulence–dominated regime with few collapses, and a spectrum consistent with the KZ solution. With an increase in nonlinearity level, we see more collapses in the field, with a flattened spectrum and departure from Gaussian statistics. At a sufficiently high nonlinearity level, collapses become more dominant, and the spectrum transitions from a power-law to an exponential form, together with the statistics returning to quasi-Gaussian. Through a spectral decomposition, we show that the exponential spectrum is due to the dominant collapse components, indicating a transition to a new "collapse turbulence" regime. This can be understood as an analogy to soliton turbulence in integrable systems, e.g., 1D Korteweg-de Vries (KdV) and focusing NLS equations, where exponential spectrum is also observed (e.g., Refs. [28,29]). We finally show that the random wave components evolve toward a thermoequilibrium state with reduced flux in the collapse turbulence regime. We remark that these findings for the focusing MMT are drastically different from the defocusing case (e.g., Refs. [18,19,21,23]), and shed light on physical systems where modulational instability-induced coherent structures are important, such as nonlinear optics, plasma waves, and deep water waves (see Ref. [30]).

II. MMT EQUATION AND NUMERICAL PROCEDURE

We consider the 1D MMT equation with focusing nonlinearity,

$$i\frac{\partial\psi}{\partial t} = |\partial_x|^{\alpha}\psi - |\partial_x|^{\beta/4}(||\partial_x|^{\beta/4}\psi|^2|\partial_x|^{\beta/4}\psi), \tag{1}$$

where $\psi(x,t)$ is a field taking complex values and the operator $|\partial_x|^{\alpha}$ denotes the multiplication by $|k|^{\alpha}$ on each component in the spectral domain. The parameter β controls the nonlinearity formulation and α controls the dispersion relation $\omega(k) = |k|^{\alpha}$ with ω the frequency and k the wave number. We set $\alpha = 1/2$ and $\beta = 0$, which aligns with the parameters used in previous studies (e.g., Refs. [16,17,20,26,27]). The MMT equation (1) conserves total action $N = \int |\psi|^2 dx$ and the Hamiltonian $H = H_2 + H_4$ with linear and nonlinear parts,

$$H_2 = \int ||\partial_x|^{\alpha/2}\psi|^2 dx,$$
$$H_4 = -\frac{1}{2}\int ||\partial_x|^{\beta/4}\psi|^4 dx. \tag{2}$$

It is shown in Refs. [16] and [17] that (1) allows a solution of wave collapse. Under the choice of $\alpha = 1/2$ and $\beta = 0$, such a solution corresponds to an integrable singularity in physical space. We summarize the theoretical argument following Refs. [16] and [17] in Appendix A, where we also point out skepticism toward procedures and suggested modifications, e.g., how the original solution can be modified to be more consistent with our numerical observations. We note that after Refs. [16] and [17], the terminology "wave collapse" is adopted in many studies (e.g., Refs. [20,26,27]) for coherent structures observed in simulations of (1), even though the correspondence is not directly established. In this paper, we will continue to use this terminology; however, the reader should keep in mind that the correspondence to Ref. [16] and [17] has yet to be established. Furthermore, the modification proposed in the Appendix A needs to be implemented in future work to improve the consistency between theory and observation.

We next present details of our simulations. Each numerical simulation is performed with 4096 modes, which corresponds to a maximum wave number of 1024 after dealiasing, on a periodic domain of $L = 2\pi$. We find that this number of modes is sufficient to capture the main discovery in this paper. This is documented in Appendix B that the use of more modes provides consistent results as presented in the main article. We start simulations of (1) from a low-amplitude background of random waves as initial conditions, and let the field evolve into a stationary state under forcing and dissipation. The forcing is in white-noise form, given by

$$F = \begin{cases} F_r + iF_i, & 4 \leqslant |k| \leqslant 13, \\ 0, & \text{otherwise}, \end{cases} \tag{3}$$

with F_r and F_i independently drawn from a Gaussian distribution $\mathcal{N}(0,\sigma^2)$. We use a broad range of $\sigma \in [0.037, 3.41]$ in the simulations to ensure that the nonlinearity level achieved covers the range of interest. We remark that alternative forcing schemes with deterministic forms (e.g., Refs. [9,19,21,31]) can also be effective.

The dissipation is imposed with the addition of two hyperviscosity terms

$$D_1 = \begin{cases} -i\nu_1\hat{\psi}_k, & |k| \geqslant 900, \\ 0, & \text{otherwise}, \end{cases}$$
$$D_2 = \begin{cases} -i\nu_2\hat{\psi}_k, & |k| \leqslant 4, \\ 0, & \text{otherwise}, \end{cases} \tag{4}$$

at small and large scales, respectively. The MMT model admits an inverse cascade; therefore, the addition of large-scale dissipation is necessary to prohibit the accumulation of energy at these scales. The dissipation coefficients are set to $\nu_1 = 10^{-14}(|k| - 900)^8$ and $\nu_2 = 3|k|^{-4}$ for all numerical experiments. We note that one can alternatively use a continuous dissipation scheme as in, e.g., Refs. [21,32]. Additional details on the numerical schemes used to solve (1) can be found in Refs. [8,14,33].

III. RESULTS

A. Spectral properties and statistics

We define $\epsilon = H_4/H_2$ in the stationary state as a measure of the nonlinearity level of the wave field and the wave action spectrum $n_k = \langle\hat{\psi}_k\hat{\psi}_k^*\rangle$ with $\hat{\psi}_k$ the Fourier transform of ψ and the angle brackets denoting an ensemble average (or time average for numerical results). Figure 1 shows the wave action spectrum n_k, as well as the corresponding wave field for three very different nonlinearity levels ranging from $\epsilon \in [0.03, 0.89]$. At a low nonlinearity level [Figs. 1(a) and 1(d)], there are few collapses in the field and the spectrum

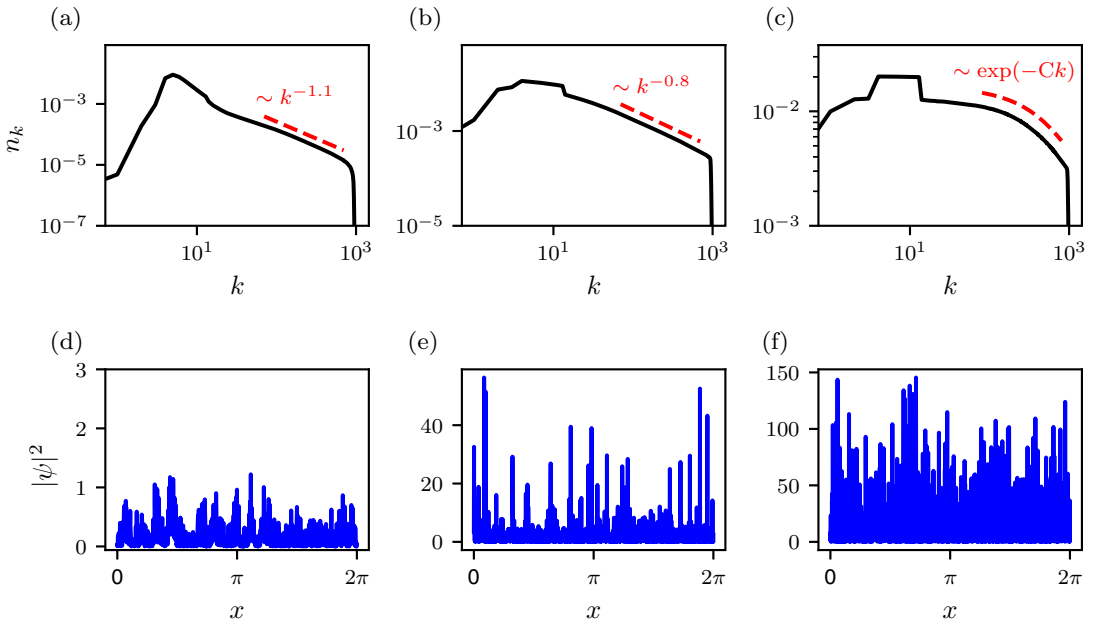

FIG. 1. (Top) Wave action spectra and (bottom) corresponding snapshots of the $|\psi|^2$ for three levels of nonlinearity with [(a) and (d)] $\epsilon = 0.03$, [(b) and (e)] $\epsilon = 0.21$, and [(c) and (f)] $\epsilon = 0.89$.

exhibits a power-law form with a slope close to the KZ prediction of $\gamma = -1$. With an increase in nonlinearity [Figs. 1(b) and 1(e)], we see more collapses emerging from the field, and the power-law spectrum becomes flatter than the KZ prediction. These observations are consistent with previous studies [19,25]. At very high nonlinearity exceeding that of previous studies [Figs. 1(c) and 1(f)], the field becomes saturated with collapses, and the wave action spectrum departs from a power law and tends toward an exponential form. We remark that such an exponential spectrum is similar to that of a soliton gas in integrable turbulence (e.g., Refs. [28,29,34,35]), where a large number of solitons exist with a background of random waves [36]. For nonintegrable systems, the only known example (to the authors) of an exponential spectrum is observed in the discrete NLS [37]. This state, involving the coexistence of waves and localized excitations, is termed a“ two-species gas.” For continuous nonintegrable systems, the authors are not aware of other examples, and the result for the MMT model is therefore a new finding.

We further investigate the wave statistics at different levels of nonlinearity. Figure 2 shows the probability distribution functions (PDFs) of $\mathrm{Re}[\psi]$ and the squared amplitude $|\psi|^2$ at the same nonlinearity levels as those in Fig. 1. At a low nonlinearity level [Figs. 2(a) and 2(b)], we see that the histogram of $\mathrm{Re}[\psi]$ is well fitted by a Gaussian distribution and $|\psi|^2$ follows an exponential distribution. At a higher level of nonlinearity [Figs. 2(c) and 2(d)], deviations from the Gaussian and exponential distributions are observed with fatter tails, indicating increased intermittency of the system. These behaviors are consistent with those observed in previous studies of the MMT model [26,27,38], as well as with general observations of intermittency in wave turbulence (e.g., Refs. [39–42]). With a further increase in nonlinearity to the level where wave collapses become dominant [Figs. 2(e) and 2(f)], we observe that the statistics of $\mathrm{Re}[\psi]$ interestingly return to being close to Gaussian (and $|\psi|^2$ to exponential). This is likely because when collapses are dominant, they become the main feature

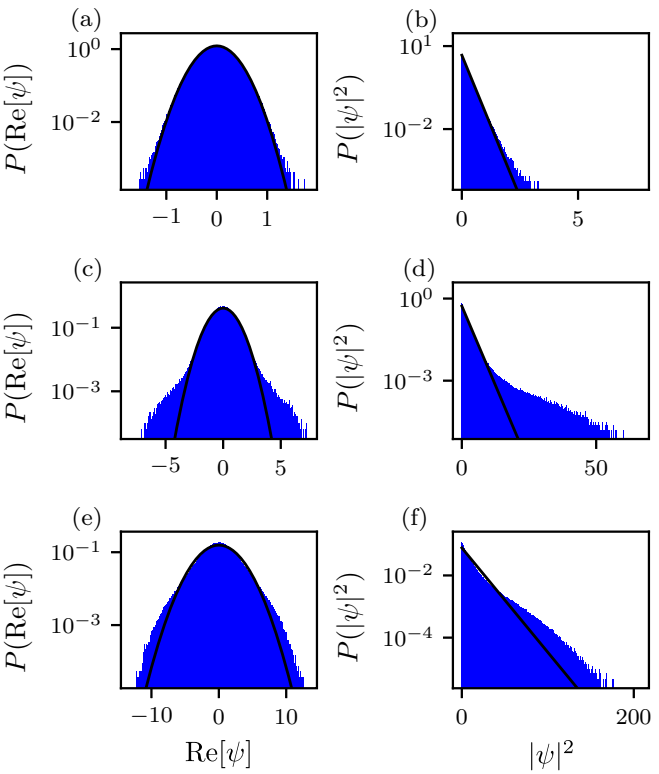

FIG. 2. Probability distributions functions of (left) $\mathrm{Re}[\psi]$ and (right) $|\psi|^2$ for three levels of nonlinearity with [(a) and (b)] $\epsilon = 0.03$, [(c) and (d)] $\epsilon = 0.21$, and [(e) and (f)] $\epsilon = 0.89$. Each panel is fitted with a Gaussian or exponential distribution of the same mean and standard deviation (solid line).

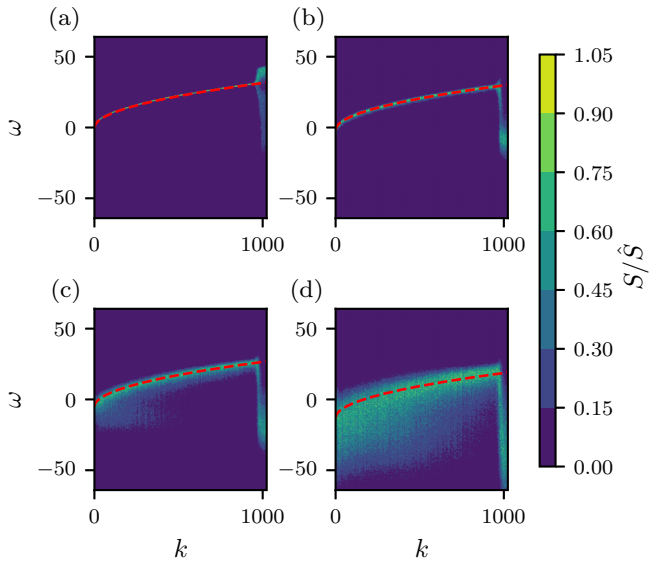

FIG. 3. The wave number–frequency spectra $S/\hat{S}$ for nonlinearity level (a) $\epsilon = 0.03$, (b) $\epsilon = 0.21$, (c) $\epsilon = 0.48$, and (d) $\epsilon = 0.89$. The red dashed lines indicate the renormalized dispersion relation $\tilde{\omega}(k)$.

of the field rather than an intermittent one. Consequently, the intermittency and non-Gaussian tail of the PDF have to be reduced.

We note that an extended self-similarity analysis (ESS) can also be performed following the procedure in Ref. [21]. Assuming structure functions $S_p \sim r^{\xi_p}$ and $S_2 \sim r^{\xi_2}$, the purpose of this analysis is to compare ξ_p/ξ_2 from numerical data with scale-invariant scaling $p/2$. Our results of this analysis (not shown) indicate that as ϵ increases from 0.03 to 0.21, ξ_p/ξ_2 departs from $p/2$ due to intermittency, consistent with Ref. [21]. As ϵ increases further to 0.89, we observe that ξ_p/ξ_2 returns to the $p/2$ scale. However, it must be emphasized that the spectrum is not a power law at high nonlinearity, violating the scaling of the structure functions as the basis of ESS. Therefore, this result needs to be interpreted with caution, which we choose not to stress in this paper.

B. Wave number–frequency spectrum and spectral decomposition

We next examine the wave number–frequency spectrum at different nonlinearity levels, as plotted in Fig. 3. Specifically, we have plotted the normalized spectrum $S/\hat{S}$, where S is the standard wave number–frequency spectrum and $\hat{S} = \max_\omega S(k, w)$. In this way, the spectral behavior at each k (especially large k) can be elucidated. Also shown in Fig. 3 are the renormalized dispersion relation curves $\tilde{\omega}(k) = \omega(k) - 2\sum_{k_1} |\hat{\psi}_1|^2$ [43] as dashed lines. At low nonlinearity [Fig. 3(a)], we see that the spectral intensity aligns well with the dispersion relation curve, suggesting the dominance of random waves in the field consistent with WTT. With an increase in the level of nonlinearity [Figs. 3(b) and 3(c)], we see spectral broadening around the dispersion relation curve, as well as the emergence of components below the dispersion relation curve, especially in Fig. 3(c). These are exact representations of the collapses that do not satisfy the

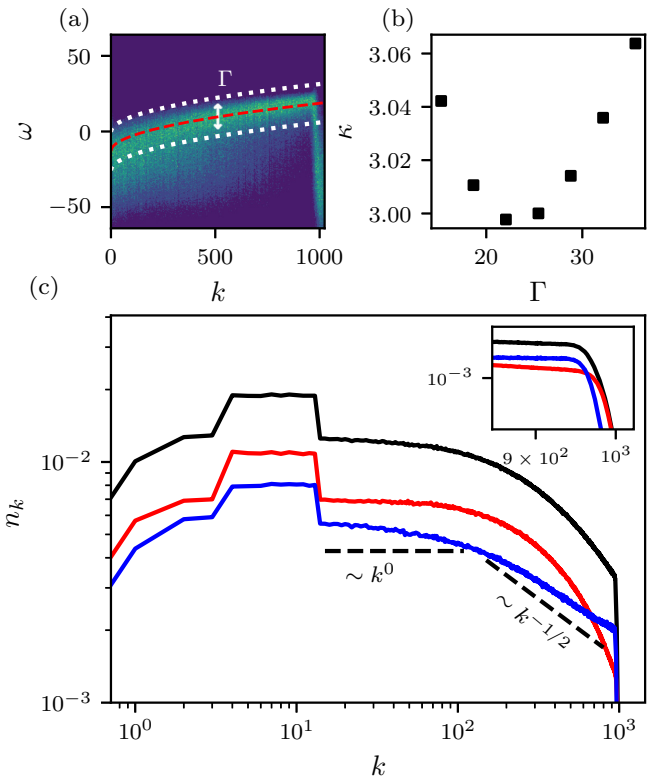

FIG. 4. Spectral decomposition for the case with $\epsilon = 0.89$. (a) an illustration of the broadening parameter Γ for defining the wave component; (b) the kurtosis κ as a function of Γ; (c) the decomposed wave action spectrum with the total spectrum (solid black), the wave component spectrum (solid blue), and the collapse component spectrum (solid red). The Rayleigh-Jeans spectra with $n_k \sim k^0$ and $n_k \sim k^{-1/2}$ are indicated by the dashed black lines. A zoomed-in view of the high-wave-number region of the spectra is included as an inset.

dispersion relation. At high nonlinearity [Fig. 3(d)], we see that the collapse component becomes more dominant, shown as signals that fill a large area in the ω-k space. We also note that in all figures, the random wave components follow the renormalized dispersion relation $\tilde{\omega}(k)$ [instead of $\omega(k) = k^{1/2}$], which is more clearly seen at higher nonlinearity. We further decompose the field at high nonlinearity $\epsilon = 0.89$ into wave and collapse components using a variation of the method developed in Ref. [44]. Generally speaking, the method decomposes the wave and collapse components according to their proximity to the dispersion relation curve. Our application of the method is described in Fig. 4. We first choose a broadening parameter Γ [see Fig. 4(a)] such that the spectral content within $\tilde{\omega}(k) \pm \Gamma/2$ satisfies a Gaussian distribution. This can be achieved by measuring kurtosis κ as a function of Γ as in Fig. 4(b), and choosing the value of Γ for which $\kappa = 3$. For our case, the optimal Γ is approximately 20–25, and we use 25 for this study. Figure 4(a) shows that such a choice of Γ roughly incorporates the major spectral content around the dispersion relation curve. We can then define the random wave component as the spectral content within $\tilde{\omega}(k) \pm \Gamma/2$, and the collapse component as the rest. Specifically, we take the inverse Fourier transform of each component, returning their respective wave fields $\psi(x, t)$ and compute the

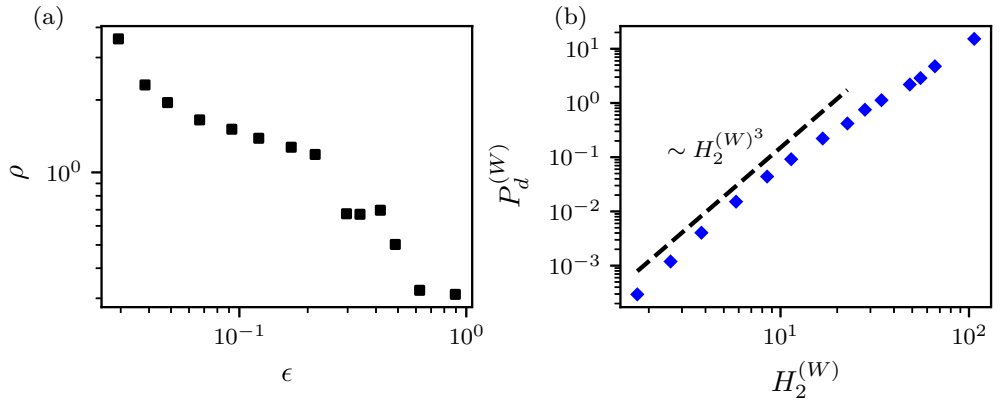

FIG. 5. (a) The ratio ρ as a function of nonlinearity level ϵ; (b) energy flux $\bar{P}_d{}^{(W)}$ as a function of $H_2^{(W)}$ for the wave component, with WTT prediction $\bar{P}_d{}^{(W)} \sim H_2^{(W)^3}$ denoted by the dashed line.

relevant decomposed quantities accordingly. Figure 4(c) shows the decomposed wave action spectra for both the wave and the collapse components. We see that the exponential total spectrum indeed results from the collapse component that is dominant for most wave numbers, with its spectrum taking an exponential form. On the other hand, the spectrum of the random wave component remains power-law form close to a thermoequilibrium state [see fitting with Rayleigh-Jeans spectrum in Fig. 4(c)], indicating that the energy flux by random waves is suppressed in the collapse-dominant regime.

We next perform a more detailed analysis of the energy flux mechanism of the system. As mentioned in Refs. [19,25,26], there are two mechanisms of energy cascade in the focusing MMT model: one local transport in k space from wave-wave interactions of random waves and the other nonlocal transport in k space from the formation of small-scale wave collapses. Therefore, the total energy flux results from the summation of the two mechanisms. Our goal is to understand the relative importance of the two mechanisms at different levels of nonlinearity. Considering that the energy flux from the two mechanisms is equal to the dissipation of random waves and collapses, respectively, we define a ratio

$$\rho = \frac{\bar{P}_d{}^{(W)}}{\bar{P}_d{}^{(C)}}, \tag{5}$$

where $\bar{P}_d{}^{(W)}$ and $\bar{P}_d{}^{(C)}$ are the dissipations of wave and collapse components, calculated as

$$\bar{P}_d{}^{*} = \sum_{k>k_d=900} -2\nu_1\omega_k n_k^*, \quad * = (W), (C), \tag{6}$$

with n_k^* decomposed as in Fig. 4(c).

Figure 5(a) plots the ratio ρ as a function of the nonlinearity level ϵ. We see a significant reduction in ρ with an increase in ϵ, indicating that the fraction of energy flux from random waves decreases substantially with increasing nonlinearity. According to this result, we conclude that the system behaves in the following way: As nonlinearity increases, the energy flux due to wave-wave interactions grows following the WTT prediction of $\bar{P}_d{}^{(W)} \sim H_2^{(W)^3}$ up to moderately high nonlinearity. Beyond this point, the energy flux from the wave component becomes lower than the WTT prediction, as seen in Fig. 5(b). This is consistent with the flattened spectrum toward the thermal-equilibrium state. This transition point occurs at approximately $\rho \lesssim O(1)$, indicating a significant portion of the contribution to the energy flux of the collapse component. Meanwhile, the energy flux from the collapse component increases much faster than that from waves, leading to a decreased value of ρ with an increase in nonlinearity as seen in Fig. 5(a).

IV. CONCLUSION

In this work, we numerically study the spectral properties and statistics of the forced-dissipated 1D focusing MMT equation, which admits wave collapses due to modulational instability. Our work covers a broader range of forcing (thus nonlinearity levels) than previous works and therefore reveals the physics at a sufficiently high nonlinearity level when wave collapses become the dominant feature. We show that as nonlinearity increases toward this collapse-dominant regime, the spectrum departs from a power-law form and tends toward an exponential form. In the meantime, the system surpasses the intermittent regime characterized by strongly non-Gaussian statistics and recovers the quasi-Gaussian statistics. The exponential spectrum resembles what is typically seen for soliton gas in integrable turbulence, but is now realized in a nonintegrable system. Through a spectral decomposition method, we show that the nature of the exponential spectrum can indeed be attributed to the dominant collapse component. With the presence of these coherent structures, the energy flux from wave-wave interactions is reduced from the prediction by WTT with the spectrum of wave component tending toward a thermoequilibrium state.

ACKNOWLEDGMENTS

The authors thank Dr. Alexander Hrabski for the insightful discussion during this work. This research was supported by the Simons Foundation (Award ID No. 651459). The computation was performed on the Great Lakes HPC Cluster provided by Advanced Research Computing (ARC) at the University of Michigan, Ann Arbor.

APPENDIX A: STRUCTURE AND FORMATION OF COLLAPSES IN THE FOCUSING MMT MODEL

We first follow Ref. [16] to write (1) in the Fourier space:

$$i\frac{\partial\hat{\psi}_k}{\partial t} = |k|^\alpha\hat{\psi}_k - \int |k_1k_2k_3k|^{\beta/4}\hat{\psi}_1\hat{\psi}_2\hat{\psi}_3^* \times \delta(k_1+k_2-k_3-k)dk_1dk_2dk_3, \tag{A1}$$

where δ denotes the Dirac delta function and $\hat{\psi}^*$ the complex conjugate of $\hat{\psi}$.

We express the wave collapse singularities by a family of self-similar solutions to (A1), written as

$$\hat{\psi}_k(t) = (t_0-t)^{p+i\epsilon}\chi(K), \tag{A2}$$

where $K = k(t_0-t)^{1/\alpha}$, $p = (\beta-\alpha+2)/2\alpha$ and ϵ is a real constant. Substituting (A2) to (A1), one obtains

$$i(p+i\epsilon)\chi + \frac{i}{\alpha}K\chi' + |K|^\alpha\chi - \int |K_1K_2K_3K|^{\beta/4} \times \chi_1\chi_2\chi_3^*\delta(K_1+K_2-K_3-K)dK_1dK_2dK_3 = 0. \tag{A3}$$

Therefore, ϵ should be chosen as an eigenvalue of (A3) with boundary conditions to be specified.

As $t \to t_0$, the solution (A2) should remain finite, which means that the dependence on t must cancel. This imposes an asymptotic behavior on $\chi(K)$:

$$|\chi(K)| \sim CK^{-\nu}, \text{ as } K \to 0. \tag{A4}$$

with $\nu = (\beta-\alpha+2)/2$. Therefore, at $t = t_0$, (A2) takes the form $|\hat{\psi}_k| \sim Ck^{-\nu}$. Due to the conservation of wave action, the integral $\int_0^\infty |\hat{\psi}_k|^2dk$ has to converge at infinity (i.e., considering the power-law solution as a high-wave-number behavior). This gives a condition $\beta > \alpha - 1$, which is shown in Ref. [16] to be consistent with a criterion of soliton instability.

Under the condition $\beta > \alpha - 1$, we have $\nu > 1/2$. Let us further analyze (A4). If $\beta < \alpha$, i.e., $\nu < 1$, then the Fourier-domain behavior (A4) corresponds to an integrable singularity in the physical domain as a wave collapse. If $\beta > \alpha$, i.e., $\nu > 1$, then the singularity is nonintegrable and is a discontinuity of the function $\psi(x)$ or its derivatives.

For our case, we have $\alpha = 1/2$ and $\beta = 0$. This leads to $p = 3/2$ and $\nu = 3/4$, so that our wave collapse corresponds to an integrable singularity in physical space. The condition $\beta > \alpha - 1$ for the finiteness of wave action is also satisfied.

The material above directly follows Refs. [16] and [17] However, we have reason to be skeptical about the proposed solution. From the method itself, first, the self-similar solution (A2) seems to be set up in an arbitray manner, e.g., the form of p. This was probably done in Zakharov's work to match the soliton instability criterion, but we do not believe this to be necessary. Evidently, modifying the form of (A2) leads to a change of (A4) (in particular, the form of ν), which changes the Fourier-domain footprint of the collapse structure. Second, the validity of the above analysis lies in the existence of a solution to (A3) with boundary conditions (A4) and $\chi(K) = 0$ as $K \to \infty$. This is not discussed in Refs. [16] and [17]. Third, the method essentially deduces the structure of the collapse based on the Fourier-domain footprint, which is not rigorous, since the map may not be unique. In addition, the integrable singularity for $\nu < 1$ can be checked with functions in the form of $f(x) = |x|^\gamma$ with $0 < \gamma < 1$. We are uncertain about the underlying basis for the nonintegrable singularity when $\nu > 1$.

Our numerical results also suggest that the solution proposed above needs to be modified (or generalized). The condition (A4) with $\nu = 3/4$ leads to a spectrum $n_k \sim k^{-3/2}$ that is steeper than the KZ solution. However, we have observed a shallower spectrum when collapses are present. The steeper spectrum $n_k \sim k^{-3/2}$ also implies that at the time of collapse, both H_2 and $|H_4|$ decrease (since H_2 takes more weight at high k and the total H is conserved). This is also in contradiction to our observation that both H_2 and $|H_4|$ surge in the simulations. Based on these observations, we believe that (A2) should be modified such that one obtains $|\chi(K)| \sim CK^{-\nu}$ with $\nu < 1/2$ (i.e., shallower spectrum). This will require us to consider a finite k space such that the finiteness of the wave action can be satisfied. Such a solution still corresponds to an integrable singularity in physical space, and one also has to consider the boundary value problem regarding (A3) to ensure that the solution exists. We leave this for future work.

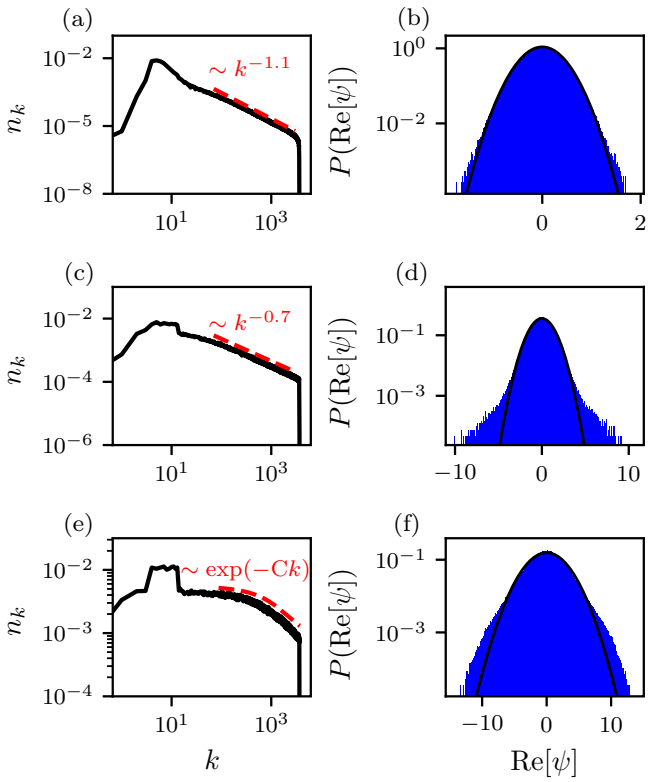

FIG. 6. (Left) Wave action spectra and (right) probability distribution fuctions of Re $[\psi]$ at three different forcing amplitudes using 16 384 modes. [(a) and (b)] $\sigma = 0.037, \epsilon = 0.019$; [(c) and (d)] $\sigma = 0.59, \epsilon = 0.13$; [(e) and (f)] $\sigma = 3.41, \epsilon = 0.50$. Each panel on the right is fitted with a Gaussian distribution of the same mean and standard deviation (solid line).

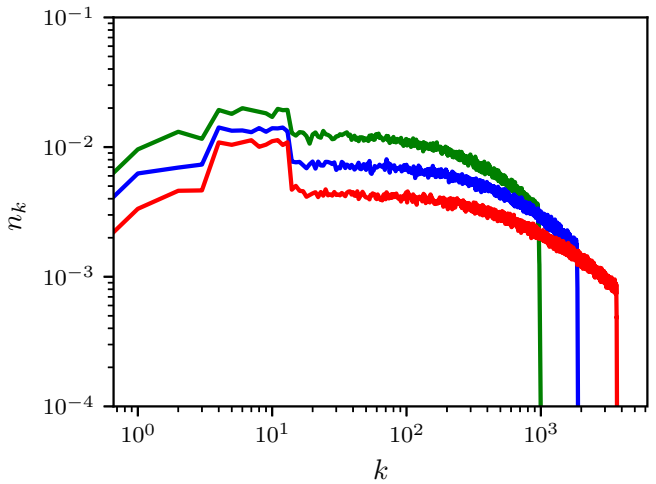

FIG. 7. The wave action spectra for 4096, $\epsilon = 0.89$ (green line); 8192, $\epsilon = 0.67$ (blue line); and 16 384, $\epsilon = 0.50$ (red line) modes. All cases have a forcing amplitude of $\sigma = 3.41$.

APPENDIX B: IMPACT OF NUMBER OF MODES

In the main paper, our numerical simulations are performed with 4096 modes, corresponding to a maximum wavenumber of 1024 after dealiasing. This leads to an inertial range of about two decades. In this Appendix, we simulate additional cases with 8192 and 16 384 modes to assess the effect of lengthening the inertial range. In all simulations, the forcing scales [i.e., (3)], dissipation parameters (i.e., ν_1 and ν_2), and domain length of $L = 2\pi$ are kept constant. The only parameter adjusted is k_d, which is set to $k_d = 1800$ and $k_d = 3600$ for cases of 8192 and 16 384 modes, respectively, so that the inertial range can be lengthened with increasing number of modes.

We first show that the main results of the paper are not affected by using more modes in the simulation. Figure 6 shows the spectrum and probability distribution of $\mathrm{Re}[\psi]$ at three different forcing amplitudes (i.e., nonlinearities) using 16 384 modes. We see that the main features detected with 4096 modes are reproduced here, in terms of the transition from power-law to exponential spectrum, as well as the deviation from and return to the Gaussian distribution.

We next study the impact of the number of modes on the spectral properties when the forcing amplitude is kept the same. Figure 7 shows the spectra with 4096, 8192, and 16 384 modes at the same forcing amplitude $\sigma = 3.41$. We see that the spectra differ from each other. This is mainly because the effective damping is different given different damping ranges, which affects the global amplitude of the spectrum. This is especially the case when constant flux is not possible as the spectrum transits toward an exponential form. As a result of this, the nonlinearity parameter ϵ also varies with the number of modes if the forcing amplitude is kept the same.

[1] S. Galtier, S. V. Nazarenko, A. C. Newell, and A. Pouquet, A weak turbulence theory for incompressible magnetohydrodynamics, J. Plasma Phys. **63**, 447 (2000).

[2] V. Zakharov and N. Filonenko, Weak turbulence of capillary waves, J. Appl. Mech. Tech. Phys. **8**, 37 (1971).

[3] V. S. L'vov, Y. L'vov, A. C. Newell, and V. Zakharov, Statistical description of acoustic turbulence, Phys. Rev. E **56**, 390 (1997).

[4] A. Picozzi, J. Garnier, T. Hansson, P. Suret, S. Randoux, G. Millot, and D. Christodoulides, Optical wave turbulence: Towards a unified nonequilibrium thermodynamic formulation of statistical nonlinear optics, Phys. Rep. **542**, 1 (2014).

[5] V. E. Zakharov, Weak turbulence in media with a decay spectrum, J. Appl. Mech. Tech. Phys. **6**, 22 (1965).

[6] A. Korotkevich, A. Pushkarev, D. Resio, and V. Zakharov, Numerical verification of the weak turbulent model for swell evolution, Eur. J. Mech. B Fluids **27**, 361 (2008).

[7] Y. Pan and D. K. P. Yue, Direct numerical investigation of turbulence of capillary waves, Phys. Rev. Lett. **113**, 094501 (2014).

[8] A. Hrabski and Y. Pan, On the properties of energy flux in wave turbulence, J. Fluid Mech. **936**, A47 (2022).

[9] Z. Zhang and Y. Pan, Numerical investigation of turbulence of surface gravity waves, J. Fluid Mech. **933**, A58 (2022).

[10] E. Falcon and N. Mordant, Experiments in surface gravity–capillary wave turbulence, Annu. Rev. Fluid Mech. **54**, 1 (2022).

[11] J. W. Banks, T. Buckmaster, A. O. Korotkevich, G. Kovačič, and J. Shatah, Direct verification of the kinetic description of wave turbulence for finite-size systems dominated by interactions among groups of six waves, Phys. Rev. Lett. **129**, 034101 (2022).

[12] Y. Zhu, B. Semisalov, G. Krstulovic, and S. Nazarenko, Testing wave turbulence theory for the Gross-Pitaevskii system, Phys. Rev. E **106**, 014205 (2022).

[13] Y. Zhu, B. Semisalov, G. Krstulovic, and S. Nazarenko, Direct and inverse cascades in turbulent Bose-Einstein condensates, Phys. Rev. Lett. **130**, 133001 (2023).

[14] A. Simonis, A. Hrabski, and Y. Pan, On the time scales of spectral evolution of nonlinear waves, J. Fluid Mech. **979**, A33 (2024).

[15] A. J. Majda, D. W. McLaughlin, and E. G. Tabak, A one-dimensional model for dispersive wave turbulence, J. Nonlin. Sci. **7**, 9 (1997).

[16] V. Zakharov, P. Guyenne, A. Pushkarev, and F. Dias, Wave turbulence in one-dimensional models, Physica D **152-153**, 573 (2001).

[17] V. Zakharov, F. Dias, and A. Pushkarev, One-dimensional wave turbulence, Phys. Rep. **398**, 1 (2004).

[18] B. Rumpf, A. C. Newell, and V. E. Zakharov, Turbulent transfer of energy by radiating pulses, Phys. Rev. Lett. **103**, 074502 (2009).

[19] D. Cai, A. J. Majda, D. W. McLaughlin, and E. G. Tabak, Spectral bifurcations in dispersive wave turbulence, Proc. Natl. Acad. Sci. USA **96**, 14216 (1999).

[20] B. Rumpf and A. C. Newell, Wave instability under short-wave amplitude modulations, Phys. Lett. A **377**, 1260 (2013).

[21] S. Chibbaro, F. De Lillo, and M. Onorato, Weak versus strong wave turbulence in the Majda-McLaughlin-Tabak model, Phys. Rev. Fluids **2**, 052603(R) (2017).

[22] R. S. Dù and O. Bühler, The impact of frequency bandwidth on a one-dimensional model for dispersive wave turbulence, J. Nonlin. Sci. **33**, 81 (2023).
[23] A. Hrabski and Y. Pan, Verification of wave turbulence theory in the kinetic limit, Phys. Rev. Res. **6**, 023184 (2024).
[24] C. Sulem and P.-L. Sulem, *The Nonlinear Schrödinger Equation: Self-focusing and Wave Collapse* (Springer Science & Business Media, New York, 2007), Vol. 139.
[25] D. Cai, A. J. Majda, D. W. McLaughlin, and E. G. Tabak, Dispersive wave turbulence in one dimension, Physica D **152-153**, 551 (2001).
[26] B. Rumpf and L. Biven, Weak turbulence and collapses in the Majda–McLaughlin–Tabak equation: Fluxes in wavenumber and in amplitude space, Physica D **204**, 188 (2005).
[27] B. Rumpf and T. Y. Sheffield, Transition of weak wave turbulence to wave turbulence with intermittent collapses, Phys. Rev. E **92**, 022927 (2015).
[28] E. Pelinovsky and A. Sergeeva (Kokorina), Numerical modeling of the KdV random wave field, Eur. J. Mech. B Fluids **25**, 425 (2006).
[29] A. A. Gelash and D. S. Agafontsev, Strongly interacting soliton gas and formation of rogue waves, Phys. Rev. E **98**, 042210 (2018).
[30] P. A. Robinson, Nonlinear wave collapse and strong turbulence, Rev. Mod. Phys. **69**, 507 (1997).
[31] A. O. Korotkevich, Inverse cascade spectrum of gravity waves in the presence of a condensate: A direct numerical simulation, Phys. Rev. Lett. **130**, 264002 (2023).
[32] Y. Pan and D. K. P. Yue, Decaying capillary wave turbulence under broad-scale dissipation, J. Fluid Mech. **780**, R1 (2015).
[33] A. Hrabski and Y. Pan, Effect of discrete resonant manifold structure on discrete wave turbulence, Phys. Rev. E **102**, 041101(R) (2020).
[34] A. Gelash, D. Agafontsev, V. Zakharov, G. El, S. Randoux, and P. Suret, Bound state soliton gas dynamics underlying the spontaneous modulational instability, Phys. Rev. Lett. **123**, 234102 (2019).
[35] I. Redor, E. Barthélemy, H. Michallet, M. Onorato, and N. Mordant, Experimental evidence of a hydrodynamic soliton gas, Phys. Rev. Lett. **122**, 214502 (2019).
[36] G. A. El, Soliton gas in integrable dispersive hydrodynamics, J. Stat. Mech. (2021) 114001.
[37] B. Rumpf and A. C. Newell, Intermittency as a consequence of turbulent transport in nonlinear systems, Phys. Rev. E **69**, 026306 (2004).
[38] W. Cousins and T. P. Sapsis, Quantification and prediction of extreme events in a one-dimensional nonlinear dispersive wave model, Physica D **280-281**, 48 (2014).
[39] Y. V. Lvov and S. Nazarenko, Noisy spectra, long correlations, and intermittency in wave turbulence, Phys. Rev. E **69**, 066608 (2004).
[40] E. Falcon, S. Fauve, and C. Laroche, Observation of intermittency in wave turbulence, Phys. Rev. Lett. **98**, 154501 (2007).
[41] E. Falcon, S. G. Roux, and C. Laroche, On the origin of intermittency in wave turbulence, Europhys. Lett. **90**, 34005 (2010).
[42] A. Alberello, M. Onorato, F. Frascoli, and A. Toffoli, Observation of turbulence and intermittency in wave-induced oscillatory flows, Wave Motion **84**, 81 (2019).
[43] S. Nazarenko, *Wave Turbulence* (Springer, Berlin, 2011).
[44] J. Laurie, U. Bortolozzo, S. Nazarenko, and S. Residori, One-dimensional optical wave turbulence: Experiment and theory, Phys. Rep. **514**, 121 (2012).